

# Thermal Fluctuations in a Lamellar Phase of a Binary Amphiphile-Solvent Mixture: a Molecular Dynamics Study.

C. Loison,<sup>1,2,\*</sup> M. Mareschal,<sup>2</sup> K. Kremer,<sup>3</sup> and F. Schmid<sup>1,†</sup>

<sup>1</sup>*Fakultät für Physik, Universität Bielefeld, Universitätsstraße 25, D-33615 Bielefeld, Germany*

<sup>2</sup>*Centre Européen de Calcul Atomique et Moléculaire, ENS Lyon, 46, Allée d'Italie, 69007 Lyon, France*

<sup>3</sup>*Max Planck Institute for Polymer Research, Ackermannweg 10, 55128 Mainz, Germany*

(Dated: version of November 9, 2018)

We investigate thermal fluctuations in a smectic A phase of an amphiphile-solvent mixture with molecular dynamics simulations. We use an idealized model system, where solvent particles are represented by simple beads, and amphiphiles by bead-and-spring tetramers. At a solvent bead fraction of 20 % and sufficiently low temperature, the amphiphiles self-assemble into a highly oriented lamellar phase. Our study aims at comparing the structure of this phase with the predictions of the elastic theory of thermally fluctuating fluid membrane stacks [Lei *et al.*, J. Phys. II **5**,1155 (1995)]. We suggest a method which permits to calculate the bending rigidity and compressibility modulus of the lamellar stack from the simulation data. The simulation results are in reasonable agreement with the theory.

## I. INTRODUCTION.

Lipids are essential components of biomembranes. Their ability to self-assemble into bilayers is characteristic for amphiphilic molecules, *i.e.*, molecules with a hydrophilic head-group and one or several hydrophobic tails. In concentrated aqueous solution, most lipids form a lamellar  $L_\alpha$  phase: a stack of amphiphile bilayers separated by layers of solvent. At room temperature, the bilayers usually have the structure of two dimensional fluids. The bilayer stack exhibits liquid-like behavior in two directions, and (quasi)-crystalline ordering in the direction perpendicular to the layers. Therefore, the  $L_\alpha$  lamellar phase can be described as a smectic liquid crystal. The bilayers are planar on average, with a well defined inter-layer spacing which can be measured by X-Ray diffraction. In addition to this positional ordering, the molecules exhibit orientational ordering perpendicular to the lamellar plane (smectic A).

From an experimental point of view, lamellar phases are useful model systems which allow to study the structure of lipid bilayers very conveniently, *e.g.* in diffraction studies. The shape of X-ray diffraction peaks has been discussed mostly in terms of the classical theory of smectic A, as developed originally by Caillé<sup>1</sup> and de Gennes,<sup>2</sup> and further elaborated by Lei *et al.*<sup>3</sup> This is a continuum approach, which operates on the mesoscopic level and describes the lamellar material as a stack of two-dimensional fluctuating layers. The free energy is taken to be an elastic energy, which penalizes local layer deformations and local deviations from the average interlayer distance. Theories of this type have been used to measure the bending constant  $K$  and the compressibility  $B$  in smectics. Applied to highly aligned experimental samples, they even allowed to calculate the bending rigidity of single bilayers, and the effective interactions between them.<sup>4</sup>

On molecular length scales, interfaces in complex fluids can also be investigated by molecular simulations.<sup>5,6,7,8,9</sup>

The simulation results can then be used to verify the validity of mesoscopic theories. For example, the phenomenological description of single bilayers in terms of a surface tension  $\gamma$  and a bending rigidity  $K_c$  has been tested for idealized amphiphile models,<sup>6</sup> and more recently even for a realistic phospholipid model.<sup>9</sup> The present work aims at extending this type of study to entire lamellar stacks of bilayers. To this end, we have performed large scale molecular dynamics simulations of a simplified coarse-grained model for binary amphiphile-solvent mixtures. This made it possible to study stacks of up to fifteen bilayers, systems large enough to be compared to the continuum theory for smectics mentioned above. A straightforward analysis, based on the direct inspection of the structure factor, failed because it requires data with a very small statistical error. We have developed an alternative, more robust method, which allowed us to extract the phenomenological parameters  $K$  and  $B$ . On large length scales, our simulation results agree well with the theory.

The paper is organized as follows: In the next section, we recall the principal features of the theory (the “discrete harmonic model”).<sup>3,10</sup> In section III, we introduce the simulation model and describe the simulation method, and section IV contains our results. There we first discuss briefly the phase behavior of our model (IV A). Then we analyze the bilayer fluctuations in a lamellar phase. The fluctuations about the mean position of each membrane give the bending energy of the bilayers, and the correlations of fluctuations between adjacent membranes yield the interactions between membranes. We summarize and conclude in section V.

## II. THEORETICAL BACKGROUND: ELASTICITY IN SMECTIC A.

Before discussing the simulations, we briefly sketch the continuum theory which we use to analyze the data. It

describes the system by a discrete set of layers, stacked in the  $z$ -direction and extending continuously in the  $(x, y)$ -plane. The average distance between layers is  $\bar{d}$ . We assume that we can parametrize each layer  $n$  by a unique height function  $z = h_n(x, y)$ , and that the molecules in a layer are perpendicular to the surface, *i.e.*, the local director is given by the layer normal. The fluctuations about the mean position of the layer are characterized by the local displacement  $u_n(x, y) = h_n(x, y) - n\bar{d}$ .

Most generally, deformations of smectics may include twist, bend, and splay modes of the director, and compression of the layers. However, the energy penalty on twist and bend modes is very high, because these modes cannot be realized at constant layer spacing. Therefore, they are effectively suppressed, and the remaining relevant deformations are the splay mode and the layer compression.<sup>2,11,12</sup> The problem can be further simplified by adopting the "discrete harmonic" approximation (DH), which has been used successfully to interpret X-ray scattering data of highly oriented lamellar phases<sup>3</sup> and to study the interfacial properties of thin films of the lamellar phase.<sup>10</sup> Here only interactions between adjacent layers are taken into consideration, and the free energy is approximated by

$$\mathcal{F}_{DH} = \sum_{n=0}^{N-1} \int_A dx dy \left\{ \frac{K_c}{2} \left( \frac{\partial^2 u_n}{\partial x^2} + \frac{\partial^2 u_n}{\partial y^2} \right)^2 + \frac{B}{2} (u_n - u_{n+1})^2 \right\}. \quad (1)$$

The first term accounts for the bending energy of individual bilayers, and the second term approximates the free energy of compression. (We note that layer bending should not be confused with the bend mode of the smectic, which is neglected here.) The elasticity of the smectic phase is thus characterized by the two coefficients  $K_c$ , the bending modulus of a single membrane, and  $B$ , the compressibility modulus. These are connected with the bulk compression modulus  $\bar{B}$  and the bulk bending modulus  $K$  by the simple relations  $B = \bar{B}/\bar{d}$  and  $K_c = K\bar{d}$ . They define the in-plane correlation length  $\xi = (K_c/B)^{1/4}$  and the characteristic smectic length  $(K/\bar{B})^{1/2}$ . The surface tension  $\gamma$  of the bilayers is taken to vanish, as in a bulk phase.

The fluctuations of  $u_n$  are most conveniently studied in Fourier space, because the Fourier modes decouple in (1) and the equipartition theorem applies. We perform continuous Fourier transformations in the  $x$ - and  $y$ -direction, and a discrete Fourier transformation in the  $z$ -direction. This gives

$$u(q_z, \mathbf{q}_\perp) = \sum_n u_n(\mathbf{q}_\perp) e^{-iq_z n\bar{d}} \quad (2)$$

$$u_n(\mathbf{q}_\perp) = \int_A d\mathbf{r} u_n(\mathbf{r}) e^{-i\mathbf{q}_\perp \cdot \mathbf{r}} \quad (3)$$

$$= \frac{1}{N} \sum_{q_z} u(q_z, \mathbf{q}_\perp) e^{+iq_z n\bar{d}}, \quad (4)$$

where  $q_z$  is the  $z$ -component of  $\mathbf{q}$  and  $\mathbf{q}_\perp$  the projection into the  $(x, y)$ -plane. In simulations, systems have finite extensions  $L_x, L_y, L_z$  and periodic boundary conditions apply. The components of the  $\mathbf{q}$ -vector then take only discrete values  $q_\alpha = k_\alpha(2\pi)/L_\alpha$  with integer  $k_\alpha$ . The maximum number of independent  $z$ -components  $k_z$  is given by the number of bilayers  $N$ .

From the equipartition theorem, one can then calculate the average amplitudes of fluctuations for large systems<sup>13</sup>

$$\langle |u(\mathbf{q}_\perp, q_z)|^2 \rangle = \frac{NL_x L_y k_B T}{2B [1 - \cos(q_z \bar{d})] + K_c q_\perp^4}. \quad (5)$$

Here and throughout, brackets  $\langle \cdot \rangle$  refer to thermal averages. Unfortunately, the statistical error of our simulation results for  $\langle |u(\mathbf{q}_\perp, q_z)|^2 \rangle$  was too large to allow for a direct comparison with Eq. (5). Therefore we resorted to studying the integrated quantities

$$s_n(\mathbf{q}_\perp) \doteq \frac{1}{N^2} \sum_{q_z} e^{iq_z n\bar{d}} \langle |u(\mathbf{q}_\perp, q_z)|^2 \rangle \quad (6)$$

$$= \frac{1}{N} \sum_{j=0}^{N-1} \langle u_j(\mathbf{q}_\perp) \cdot u_{n+j}(\mathbf{q}_\perp)^\dagger \rangle. \quad (7)$$

The quantity  $s_0(\mathbf{q}_\perp)$  describes correlations within membranes, whereas  $s_n(\mathbf{q}_\perp)$  (at  $n > 0$ ) characterizes correlations between membranes. In an infinitely thick stack of  $N \rightarrow \infty$  bilayers, the sum  $\sum_{q_z}$  can be replaced by the integral  $(N\bar{d}/2\pi) \int_0^{2\pi/\bar{d}} dq_z$ . Inserting Eq. (5), we obtain

$$s_0(q_\perp) \stackrel{N \rightarrow \infty}{\doteq} \frac{L_x L_y k_B T}{K_c q_\perp^4} \left[ 1 + \frac{4}{(\xi q_\perp)^4} \right]^{-1/2}, \quad (8)$$

$$s_n(q_\perp) \stackrel{N \rightarrow \infty}{\doteq} s_0(q_\perp) \times \left[ 1 + \frac{X}{2} - \frac{1}{2} \sqrt{X(X+4)} \right]^n \quad (9)$$

where  $\xi$  is the in-plane correlation length,  $\xi = (K_c/B)^{1/4}$ , and the ratios  $s_n/s_0$  between cross-correlations  $s_n$  of membranes and the autocorrelation  $s_0$  depend only on the dimensionless parameter  $X = (\xi q_\perp)^4$ . In deriving Eqs. (8) and (9), we have made use of the formula

$$\frac{1}{2\pi} \int_0^{2\pi} d\tau \frac{e^{in\tau}}{a - \cos(\tau)} = \frac{(a - \sqrt{a^2 - 1})^n}{\sqrt{a^2 - 1}}, \quad (10)$$

which can be derived by substituting  $z = e^{i\tau}$  and applying the residuum theorem.

Two regimes are expected with a crossover at  $q_c \sim \xi^{-1}$ . If  $q_\perp$  is much larger than  $q_c$ , the fluctuation spectrum  $s_0$  of single membranes is proportional to  $q_\perp^{-4}$ . This corresponds to the well-known spectrum of single isolated membranes without surface tension. The relative amplitudes  $s_n/s_0$  of cross-correlations between different layers decay exponentially like  $(1/X)^n$  with the distance  $n\bar{d}$  between the bilayers. In the small-wavelength regime, fluctuations of different membranes are thus basically incoherent, and the bilayers behave like free, unconstrained membranes.

In contrast, the regime  $q_{\perp} \ll q_c$  is dominated by the coupling of compression modes with the bending fluctuations. The ratios  $s_n/s_0$  tend towards one in the infinite wavelength limit  $X \rightarrow 0$ , *i.e.*, fluctuations of different bilayers are coherent. The fluctuation spectrum is proportional to  $q_{\perp}^{-2}$ . The fluctuations thus grow more slowly with the wavelength than those of free membranes, due to the fact that the membranes are constrained in the stack.

These results allow one to derive the height-height correlation function, which has often been used to discuss X-ray scattering spectra<sup>3,14,15</sup>  $\langle \delta u_n(r)^2 \rangle$  with

$$\delta u_n(x, y)^2 \doteq \frac{1}{N} \sum_{j=0}^{N-1} |u_{n+j}(x, y) - u_j(0, 0)|^2. \quad (11)$$

This quantity can be calculated from back transforming the  $s_n(q_{\perp})$  into the real space  $(x, y)$ . One obtains

$$\langle \delta u_n(r)^2 \rangle = \frac{2\eta_1}{q_1^2} \int_0^{\infty} d\tau \frac{1 - J_0\left(\frac{r}{\xi} \sqrt{2\tau}\right) [\sqrt{1 + \tau^2} - \tau]^{2n}}{\tau \sqrt{1 + \tau^2}}, \quad (12)$$

where  $r = \sqrt{x^2 + y^2}$ ,  $J_0$  is the first Bessel function,  $q_1$  the position of the first diffraction peak ( $q_1 = 2\pi/\bar{d}$ ), and  $\eta_1$  is the Caillé parameter<sup>1</sup>

$$\eta_1 = \frac{k_B T}{8\sqrt{BK_c}} \frac{4\pi}{d^2}. \quad (13)$$

The Caillé parameter is often used to characterize the width of diffraction peaks. Within the elastic theory (1), it can be determined easily, since all height-height correlations are proportional to  $\eta_1$ .

### III. MODEL AND METHOD.

#### A. The simulation model.

Our simulation model is based on a coarse-grained off-lattice model, which has been used extensively for polymers,<sup>16,17,18</sup> and was recently optimized to study rheologic properties of amphiphilic dimers.<sup>19,20</sup>

All molecules are represented by one or several soft beads (for simplicity, all beads are taken to have the same size  $\sigma$  and the same mass  $m$ ). The solvent is represented by single soft spheres (type *s*). One solvent bead represents roughly three water molecules (the simulations could also be compared to amphiphiles in an oily solvent. In that case, one bead would correspond to one propane molecule, or to a portion of a bigger alkane). The amphiphilic molecules are linear tetramers composed of two solvophobic beads (or "tail beads", denoted *t*) and two solvophilic beads (or "head beads", denoted *h*). The soft spheres of the amphiphilic  $h_2t_2$  are covalently bonded.

Non-bonded beads interact with short ranged poten-

tials of the form (see Fig. 1 A for an illustration)

$$U_{LJ-cos}(r) = \begin{cases} 4\epsilon \left[ \left(\frac{\sigma}{r}\right)^{12} - \left(\frac{\sigma}{r}\right)^6 + \frac{1}{4} \right] - \phi & \text{if } r \leq 2^{1/6}\sigma \\ \frac{\phi}{2} [\cos(\alpha r^2 + \beta) - 1] & \text{if } 2^{1/6}\sigma \leq r \leq r_c \\ 0 & \text{if } r_c \leq r \end{cases} \quad (14)$$

where  $\sigma$  is our unit of length and  $\epsilon$  our unit of energy. The potentials comprise a Lennard-Jones type soft repulsive part, and a short-ranged attractive part. The parameters  $\alpha$  and  $\beta$  are fixed such that potentials and forces are continuous everywhere. ( $\alpha = \pi/r_c^2 - 2^{1/3}\sigma^2$  and  $\beta = 2\pi - r_c^2\alpha$ ). The energetic parameter  $\phi$  determines the depth of the potential and the energetic parameter  $\epsilon$  determines the strength of the soft repulsive core. At  $\phi = 0$ , the interaction is purely repulsive. The potential depth  $\phi$  of the pair interactions is the same for all pairs of beads which "like" each other (*ss*, *sh*, *hh*, and *tt*), and zero for pairs which "dislike" each other (*ts* and *th*). For a fixed  $\epsilon$ , the self-assembly is driven by the single energetic parameter  $\phi$ . Unless stated otherwise, the parameter value for the pairs *ss*, *sh*, *hh*, and *tt* is  $\phi = 1.1\epsilon$ . The range  $r_c$  of the potential is chosen  $r_c = 1.5\sigma$ .

Bonded beads are connected by springs with the spring potential (see fig. 1 B)

$$U_{LJ-FENE}(r) = \begin{cases} 4\epsilon \left[ \left(\frac{\sigma}{r}\right)^{12} - \left(\frac{\sigma}{r}\right)^6 \right] - \left(\frac{\kappa r_b^2}{2\sigma^2}\right) \ln \left[ 1 - \left(\frac{r}{r_b}\right)^2 \right] & \text{if } r \leq r_b \\ \infty & \text{if } r_b \leq r \end{cases} \quad (15)$$

named finite extendable nonlinear spring potential (FENE). The bond parameters were fixed at  $r_b = 2.0\sigma$  and  $\kappa = 7.0\epsilon$ .

No chemical details are incorporated in the model. In particular, it contains no long-range interactions, and no chain stiffness.

In the following, lengths shall be given in units of  $\sigma$ , energies in units of  $\epsilon$  and masses in units of  $m$ . This gives the time unit  $\tau = (m\sigma^2/\epsilon)^{1/2}$ . Typical orders of magnitude of our units are  $\epsilon \sim 5 \cdot 10^{-21}$  J,  $m \sim 10^{-25}$  kg,  $\sigma \sim 5\text{\AA}$ , and  $\tau \sim 10^{-12}$  s.

As has been discussed by Soddemann *et al.*,<sup>19</sup> this coarse-grained model is simple enough that it permits to simulate very large systems. In the present work, a smectic phase composed of up to fifteen bilayers, containing several thousands of molecules each, was simulated over about  $10^5\tau$  (about 100 ns). Previous coarse-grained or all-atom simulations of bilayers or smectic phases<sup>9,21,22,23,24,25,26</sup> have been limited to smaller system sizes or simulation times, which were not sufficient to study layer interactions in the smectic phase. Schick and coworkers<sup>5,27,28</sup> have investigated one or more polymeric bilayers of similar sizes as in the present article, but they focused on the formation of pores in the bilayers or fusion between bilayers. As an alternative, lattice simulations have proven very successful to reproduce amphiphilic phases.<sup>29,30,31</sup> Compared to these, our model

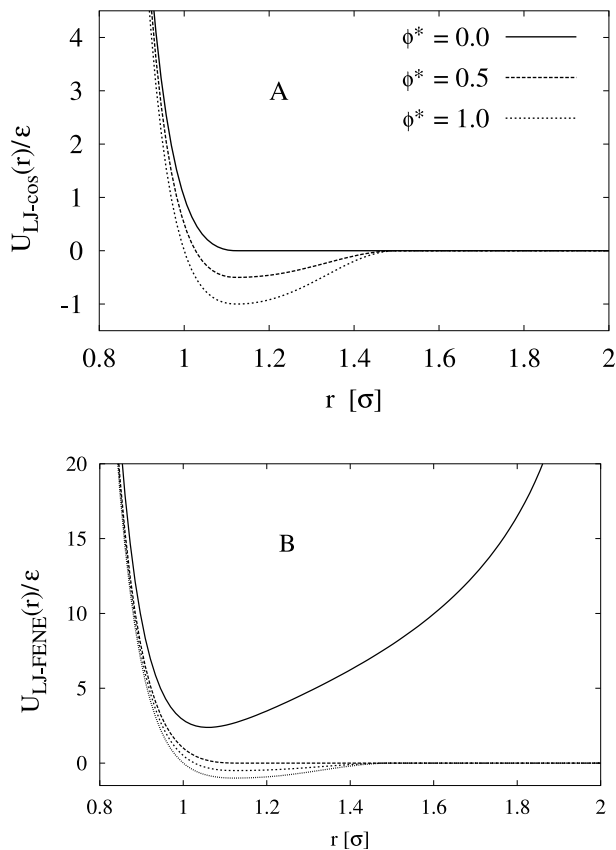


FIG. 1: Pair Potentials used in the simulations as a function of the inter-particle distance in units of  $\sigma$ . **A**): Non-bonded interactions  $U_{LJ-cos}$  for three choices of the potential depth  $\phi$  ( $\phi^* = \phi/\epsilon$ ). By construction, the position of the minimum ( $r = 2^{1/6} \sigma$ ) and the cut-off ( $r_c = 1.5 \sigma$ ) are independent of the potential depth. **B**): Bonded interactions between connected beads  $U_{LJ-FENE}$  (solid line). The minimum is located at  $r = 1.06 \sigma$ . Dashed and dotted line show the non-bonded potentials for comparison.

avoids lattice artifacts and permits to control more easily the surface tension of the bilayers.

Smectic phases can also be studied with standard coarse-grained models for liquid crystals, such as spherocylinders or Gay-Berne particles. These systems exhibit smectic A phases, which are similar to our lamellar phase. Otherwise, the phase diagram is rather different. Liquid crystal models often display a smectic/nematic phase transition, which is not present in our model (nor in real amphiphilic systems). Instead, our model exhibits an anisotropic sponge phase, and a micellar phase at low amphiphile concentrations. Nevertheless, we expect that our main results on thermal fluctuations in the lamellar phase are also valid for general smectic phases.

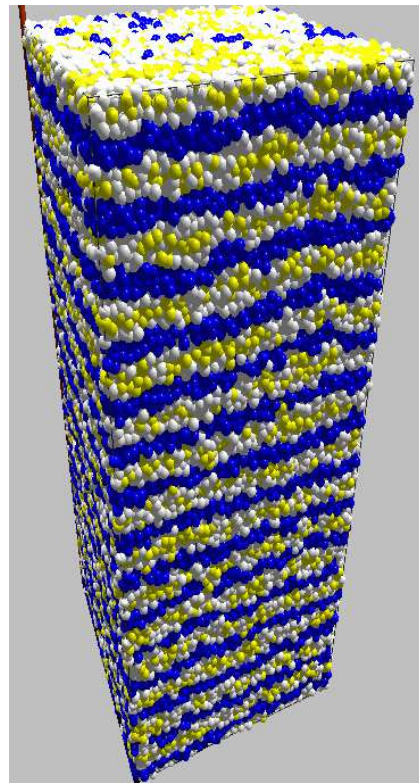


FIG. 2: Snapshot of a conformation of 30 720  $h_2t_2$  tetramers and 30 720 solvent beads, simulated in the  $NP_nP_tT$  ensemble. ( $P^* = 2.9$ ,  $T^* = 1.0$ ,  $\phi^* = 1.1$ ). The dark beads are solvophobic (type  $t$ ), the light beads are solvophilic beads or solvent beads (type  $h$  or  $s$ ).

## B. Simulation details.

We have studied the model in the  $(NP_nP_tT)$ -ensemble (constant number of particles, constant pressure normal and tangential to the bilayers, and constant temperature) with molecular dynamics simulations.

( $N$ ): The lamellar phase was studied at an amphiphile fraction of 80% of the beads (one solvent bead per  $h_2t_2$ ). Two system sizes were compared in order to detect finite size effects. The small system contained 10 240 tetramers and 10 240 solvent beads, which formed five bilayers of about two thousand molecules each. The bigger system was three times larger in the direction of the director and contained fifteen bilayers. The thermal-averaged box dimensions were  $L_x = L_y = 43.4 \pm 0.1 \sigma$ ,  $L_z = 95.7 \pm 0.2 \sigma$  for the system of fifteen bilayers and  $L_z = 31.9 \pm 0.1 \sigma$  for the system of five bilayers.

( $P$ ): The normal and tangential pressure component  $P_n$  and  $P_t$  were kept constant using the extended Hamiltonian method of Andersen.<sup>32,33</sup> The box shape is constraint to remain a rectangular parallelepiped. The box dimension perpendicular to the bilayer ( $L_z$ ) and tangential to the bilayers ( $L_x, L_y$ ) are coupled to two separated pistons. We imposed separately the two pressure components rather than the total pressure  $P = (P_n + 2P_t)/3$

because of technical reasons: the mechanical equilibrium is reached earlier, the orientation of the bilayers is stabilized, and the surface tension is controlled. Since we studied a bulk lamellar phase, we imposed an isotropic pressure ( $P_n = P_t = P$ ). More details on the simulation algorithm and simulation parameters are given in the appendix A.

( $T$ ): The temperature was controlled with a stochastic Langevin thermostat, which has been described earlier and applied to simple and complex fluids by one of us (with coworkers).<sup>18,19,34</sup> The Langevin thermostat leads to the correct temperature and to the correct canonical distributions of static observables. Therefore the thermal fluctuations appearing at thermal equilibrium can be studied using such a thermostat.

We define the dimensionless pressure  $P^* = Pk_B T/\epsilon$ , the dimensionless temperature  $T^* = k_B T/\epsilon$  and the dimensionless potential depth  $\phi^* = \phi/\epsilon$ . We have chosen to fix  $P^* = 2.9$  and  $T^* = 1.0$ . For the typical value  $\phi^* = 1.1$  the densities vary around 0.85 beads per unit volume.

With our typical parameters, lamellae form and order spontaneously (see next section). However, this process requires at least 30 000  $\tau$  in the  $NP_n P_t T$  ensemble. In most runs, we have therefore imposed the orientation of the lamellae to the initial configurations. They were constructed such that five or fifteen bilayers, separated by solvent layers with always the same number of solvent particles, were stacked in the  $z$ -direction. These configurations were then relaxed for 10 000  $\tau$ . During that time, the interlamellar distance adjusted to its equilibrium value, the shape of the flexible box changed accordingly, but the director remained basically aligned with the  $z$ -direction. Fig. 2 shows a snapshot of a large system (30 720 tetramers and 30 720 solvent beads). Data for the fluctuation analysis were then collected over 100 000  $\tau$  for both system sizes. We verified that the pressure tensor obtained at equilibrium was diagonal and isotropic: for example, in the simulation of the large system ( $P^* = 2.9$ ,  $T^* = 1.0$ ,  $\phi^* = 1.1$ ), the averages of the non-diagonal components were smaller than the errors of the computation (0.01).  $\langle \mathcal{P}_{xy} \rangle = 0.002$ ,  $\langle \mathcal{P}_{xz} \rangle = 0.002$ ,  $\langle \mathcal{P}_{yz} \rangle = -0.008$ ,  $\langle \mathcal{P}_{xx} \rangle = 2.896$ ;  $\langle \mathcal{P}_{yy} \rangle = 2.895$ , in units of  $\epsilon/\sigma^3$ . We also verified that the ensemble-averaged surface tension  $\gamma = \langle L_z(P_n - P_t) \rangle$  was negligible ( $\gamma = -0.01 \pm 0.01 \epsilon \cdot \sigma^{-2}$  per bilayer in the large system).

#### IV. RESULTS.

We shall first establish the relevant parts of the phase diagram of the model, and then discuss the layer fluctuations in the smectic phase. The behavior of a pure amphiphile system without solvent has been studied earlier by Guo and one of us.<sup>35,36</sup> Here we consider systems with solvent particles (20 % solvent particles unless stated otherwise).

##### A. Smectic ordering.

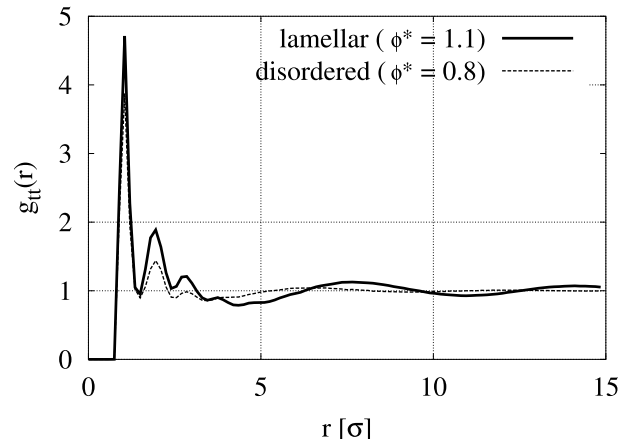


FIG. 3: Pair correlation function  $g_{tt}(r)$  of tail beads ( $t$ ), as a function of the distance  $r$  in units of  $\sigma$  measured in a system of 10 240 amphiphiles  $h_2t_2$  and 10 240 solvent beads ( $P^* = 2.9$ ,  $T^* = 1.0$ ). The two curves correspond to state points in the disordered phase ( $\phi^* = 0.8$ , dashed line) and in the lamellar phase ( $\phi^* = 1.1$ , solid line).

Fig. 3 shows the pair correlation function of tail beads  $g_{tt}(r)$  in a disordered and in a lamellar state. At short distances, it is dominated by the local liquid structure in both cases. The difference between the two structures becomes apparent at intermediate distances: The pair correlation function exhibits small oscillations in the lamellar phase with a periodicity corresponding to the inter-layer distance which are not present in the disordered phase.

The smooth structure of the fluid on intermediate length scales indicates the presence of a smectic phase and is usually analyzed in terms of a set of two order parameters: (i) The nematic order parameter, which characterizes the orientational symmetry breaking, and (ii) a smectic order parameter, which describes the breaking of translational symmetry.

The nematic order parameter  $S$  is the largest eigenvalue of the nematic order tensor  $\hat{Q}$

$$\hat{Q}_{\alpha,\beta} = \frac{1}{2N} \sum_{i=1}^N (3u_{i\alpha}u_{i\beta} - \delta_{\alpha\beta}) \quad \text{with } \alpha, \beta \in \{x,y,z\} \quad (16)$$

where the  $\mathbf{u}_i$  are unit vectors pointing in the direction of the molecules  $i$ , and the sum runs over all  $N$  molecules.<sup>2</sup> The eigenvector corresponding to the eigenvalue  $S$  is the director  $\mathbf{n}$ . In our analysis, we calculated  $\mathbf{u}_i$  from the direction of the middle bond of the molecules. Other choices are also possible and lead to similar results.<sup>37</sup> In particular, the dimensionless potential depth  $\phi^*$  at the order-disorder transition does not depend on the details of the analysis. Fig. 4 shows  $S$  as a function of  $\phi^*$  for a set of runs where  $\phi^*$  was increased from 0.82 to 1.1 in steps

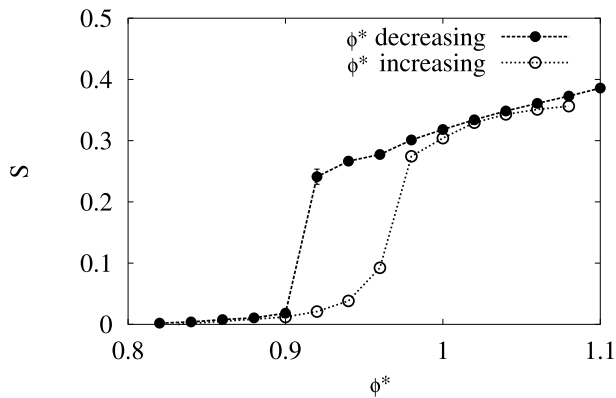


FIG. 4: Nematic order parameter  $S$  as a function of dimensionless depth  $\phi^*$  ( $P^* = 2.9$ ,  $T^* = 1.0$ ) in a system of 10 240  $h_2t_2$  tetramers and 10 240 solvent beads. The relative depth  $\phi^*$  was varied from 0.9 to 1.1 and back in steps of 0.02. At each step, the configuration was relaxed over 5 000  $\tau$  and the order parameter was then calculated over 5 000  $\tau$ . At the ordered side of the transition, the configurations still contain some linear defects after 10 000  $\tau$ . Therefore, the order parameter given here is slightly lower than the equilibrium value. The lines are guides for the eye.

of 0.02, and then reduced again. The order parameter jumps from about 0 to 0.38 when the potential depth  $\phi^*$  is increased, and back to zero when  $\phi^*$  is reduced. Hysteresis is observed. This indicates the presence of a first order phase transition between the disordered phase and an ordered phase. We did not determine precisely the parameter  $\phi^*$  of the transition. Nevertheless, Fig. 4 clearly shows that the state under investigation ( $\phi^* = 1.1$ ) is in the lamellar phase domain.

The translational symmetry breaking can be investigated by inspection of the density-density correlations along the director  $\mathbf{n}$ . We divide the system into slabs of thickness  $\Delta z$  in the direction  $z$  of the director, and calculate the density correlations of solvophobic particles (t-beads) using

$$p_{tt}(z) = \frac{1}{N_t(N_t - 1)} \times \sum_{i \neq j} \frac{1}{\Delta z} \int_{-\frac{\Delta z}{2}}^{\frac{\Delta z}{2}} dz' \delta \left( \frac{|z_i - z_j| - [z + z']}{L_z} \right) \quad (1.7)$$

Here  $N_t$  is the number of  $t$ -beads,  $z_i$  and  $z_j$  are the  $z$ -coordinates of the beads  $i$  and  $j$ ,  $L_z$  is the box dimension in the  $z$ -direction, and  $\delta$  denotes the delta function. Fig. 5 shows the resulting density correlation function for a lamellar state point in the directions parallel and perpendicular to the director. The translational symmetry is clearly broken in the direction of the director ( $z$ ), and preserved in the other two ( $x, y$ ). The density oscillations happen to be fitted nicely by a cosine function,  $f(z) = 1 + \alpha \cos(2\pi z/\bar{d})$ . The period  $\bar{d}$  corresponds to the mean inter-layer distance. As shown in Fig. 6, it increases almost linearly with the segregation factor  $\phi^*$ .

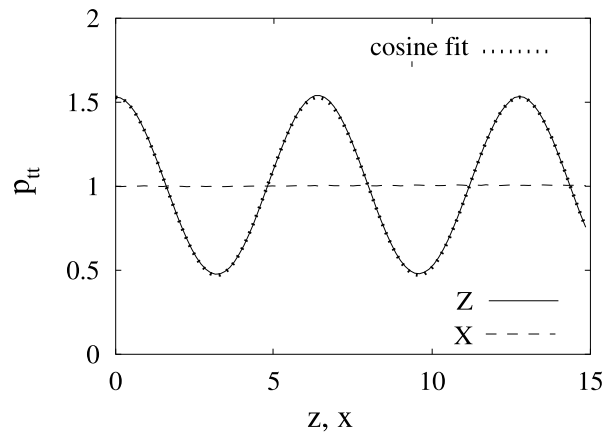


FIG. 5: Density correlation functions of tail beads in the lamellar phase ( $P^* = 2.9$ ,  $T^* = 1.0$ ,  $\phi^* = 1.1$ ) in the direction  $x$  (thin dotted line) and  $z$  (thick solid line). The correlation in  $z$ -direction is fitted by the function  $f(z) = 1 + \alpha \cos(2\pi z/\bar{d})$  with  $\alpha = 0.52$  and  $\bar{d} = 6.38 \sigma$  (thick dashed line).

The amplitude  $\alpha$  is the order parameter of the translational order. It is shown as a function of  $\phi^*$  and compared with the nematic order parameter  $S$  in Fig. 7. Both order parameters are non-zero in the ordered phase, and jump to zero simultaneously at  $\phi^* \sim 0.92$ . As expected for amphiphilic systems,<sup>19,38</sup> our model does not exhibit a separate nematic phase.

We have investigated partially the region of stability of the lamellar phase. At the number density of about 0.85 beads per unit volume (which is the density of a monomeric fluid at the dimensionless pressure  $P^* = 3.0$ ), a pure system of amphiphiles orders into a lamellar phase at  $\phi^* = 0.77 \pm 0.1$ . In contrast, a system which contains 20 % solvent beads remains lamellar only down to  $\phi^* \sim 0.98$  (see Fig. 4). The solvent destabilizes the lamellar phase. At fixed  $\phi^* = 1.1$ , the maximum amount

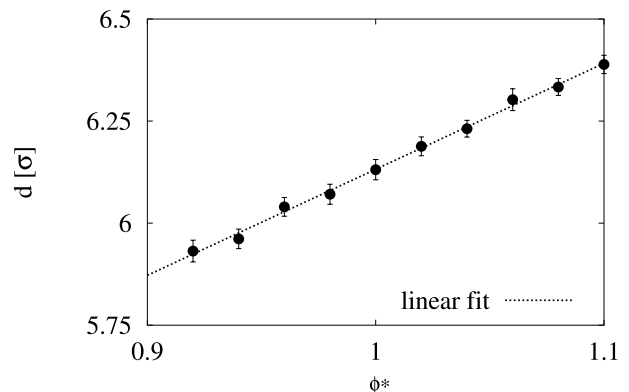


FIG. 6: Inter-layer distance  $\bar{d}$  in units of  $\sigma$  as a function of potential depth  $\phi^*$ , calculated from the simulation runs with decreasing  $\phi$  of Fig. 4. The line is a linear fit.

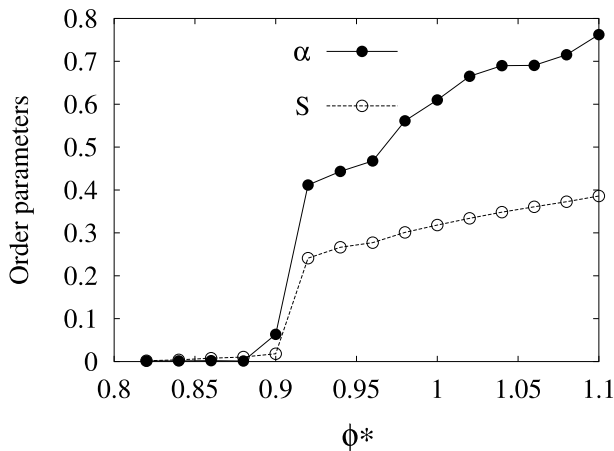


FIG. 7: Positional order parameter  $\alpha$  and orientational order parameter  $S$  as a function of potential depth  $\phi^*$ . The data correspond to the simulation runs with decreasing  $\phi^*$  of Fig. 4.

of solvent beads that could be added to the lamellar stack without destroying the smectic order was found to be roughly 40 %.

The main simulations were then carried out at a solvent volume fraction of 20 % and  $\phi^* = 1.1$ , which is well in the smectic phase. The bead density  $\rho = 0.85 \sigma^{-3}$  was maintained by applying the pressure  $P^* = 2.9$ . The local structure of the smectic layers can be characterized by the profiles of head, tail, and solvent bead densities. Unfortunately, the calculation of density profiles is hampered by the fact that the local positions of the membranes fluctuate both in time and space. To account for these effects, we have calculated the local positions of each membrane on a grid in the  $(x, y)$  plane of mesh size  $1.3\sigma$ , and evaluated local profiles in the  $z$ -direction relative to those positions, which were then averaged. The procedure is described in more detail in the next section and in appendix B. The resulting density profiles are shown in Fig. 8. The solvophobic and the solvophilic beads are well segregated. In particular, almost no solvent particles penetrate into the amphiphilic bilayers.

### B. Fluctuation analysis.

We now turn to investigate the layer fluctuations in the lamellar phase. For the fluctuation analysis, we have determined the local positions of the membranes in every configuration from the local densities of solvophobic beads. A volume element is considered to be part of a membrane, if the local density of solvophobic beads there exceeds a certain pre-defined threshold (between 0.65 and 0.75). We characterize the  $n$ th membrane by its position  $h_n(x, y)$  and its thickness  $t_n(x, y)$  (Monge representation).<sup>13</sup> In practice, only discrete values of  $x$  and  $y$  were considered ( $x = n_x L_x / N_x$  and  $y = n_y L_y / N_y$ ).

For each point  $(x, y)$ , the position and thickness of a membrane were determined as the mean and the difference of the two  $z$  values where the local density of solvophobic beads crosses the threshold value. The algorithm is described in appendix B. The displacement of the layer was then defined as  $u_n(x, y) = h_n(x, y) - \bar{h}_n$ , where the mean position  $\bar{h}_n$  was determined separately in each configuration ( $\bar{h}_n = \sum_{x,y} h_n(x, y) / (N_x N_y)$ ). The two dimensional Fourier transform of  $u_n(x, y)$  gives the fluctuation spectrum (cf. Eq. (3)). Fig. 9 shows a typical membrane configuration.

First, we analyze the distribution of inter-layer distances  $\sum_n \langle |h_n(x, y) - h_0(x, y)| \rangle$ . The histogram for the system of 15 layers is shown in Fig. 10. The periodic arrangement of the peaks reflects the smectic order of the membranes along the director - the  $n$ th peak corresponds to the distance between bilayers which are separated by  $n$  layer(s) of solvent. For each peak, the mean and the variance were determined by fitting a Gaussian function. The results are plotted as a function of  $n$  in Figs. 11 and 12. Not surprisingly, the mean distance is proportional to  $n$ ,  $\langle |h_n(x, y) - h_0(x, y)| \rangle = n\bar{d}$  with  $\bar{d} = 6.38\sigma$ . The variances reflect the height-height fluctuations (cf. Eq. (12)). From the width of the first peak, we calculated the value of the Caillé parameter,  $\eta_1 = 0.053$ . The variances of the higher order peaks are compared with the prediction of the continuous theory in Fig. 12. The theory describes the simulation data very well for small  $n$ . At large  $n$ , small discrepancies are observed, which are presumably due to finite size effects: In infinite systems,  $\langle \delta u_n(0)^2 \rangle$  should increase monotonously with  $n$ . In a finite system with periodic boundary conditions, however, it is bound to decrease beyond  $n = N/2$  and reaches zero for  $n = N$ .

Figs. 11 and 12 also display results for systems with 5 layers. The interlamellar distance does not depend significantly on the system size. The variances are re-

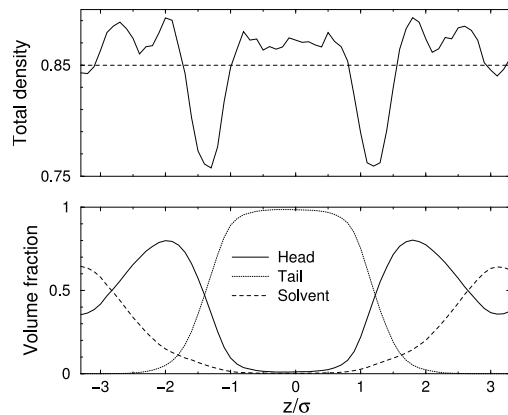


FIG. 8: Total density profiles (top) and partial volume fractions of head, tail and solvent beads (bottom) across a smectic layer ( $P^* = 2.9$ ,  $T^* = 1.0$ ,  $\phi^* = 1.1$ ). See text for more explanation.

duced in the small system, due to the finite size effect discussed above. As a consequence, the Caillé parameter  $\eta_1$  is slightly underestimated ( $\eta_1 = 0.051$ ), though still of the correct order of magnitude.

Next we study fluctuations and correlations of membranes in the  $(x, y)$  direction, which we characterize by the quantities  $s_n(\mathbf{q}_\perp)$  defined in Eq. (6) ( $q_\perp^2 = q_x^2 + q_y^2$ ). Fig. 13 shows  $s_n(\mathbf{q}_\perp)/(L_x L_y)$  for  $n = 0, 1, 2$  as a function of  $q_\perp$ .

Unfortunately, a meaningful comparison of the continuum theory and the simulation data was only possible for intermediate wavevectors  $q_\perp$ . Large wavelength fluctuations could not be analyzed reliably because the autocorrelation time for these modes ( $q_\perp = 0.1 \sigma^{-1}$ ) became comparable to the total length of the simulation run ( $100\,000 \tau$ ), even in the small system ( $N = 5$  bilayers). The correlation time drops to  $2\,500 \tau$  for  $q_\perp = 0.3 \sigma^{-1}$ . On the short wavelength side of the spectrum, the continuum theory (1) breaks down on molecular length scales. Beyond  $q_\perp \geq 1 \sigma^{-1}$ , the fluctuations of the membrane thickness have been found to follow a  $1/q_\perp^2$  behavior.<sup>9</sup> This has been interpreted in terms of an effective surface tension caused by the protrusion of molecules out of the bilayer. In our system, the protrusion regime is found at  $q \simeq 0.8 \sigma^{-1}$  (data not shown), corresponding to a length scale of about  $8 \sigma$ .

For these reasons, we shall restrict our data analysis to the  $q_\perp$  regime  $0.3 \sigma^{-1} \leq q_\perp \leq 0.8 \sigma^{-1}$  in the following.

The direct fit of Eq. (8) to the data for  $s_0(q_\perp)$  in this regime was not very significant. Comparing the ratios  $s_1/s_0$  and  $s_2/s_0$  to the theoretical prediction (9) turned out to be much more rewarding. In the big system (fifteen bilayers), the agreement between our data and the theory is very good (see Fig. 14). We have fitted the results for  $s_1/s_0$  and  $s_2/s_0$  independently, with only one fit parameter  $\xi$ . Both fits give the same values within the errors,  $\xi = 2.34 \pm 0.01 \sigma$ . In the small system (five bilayers), the infinite slab approximation  $N \rightarrow \infty$  be-

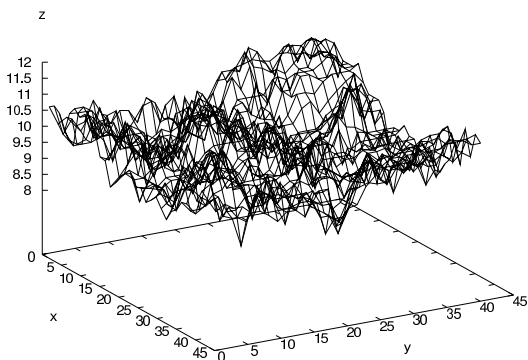


FIG. 9: Typical conformation of the position  $h_n(x, y)$  of a membrane in a stack of five membranes. See text and appendix B for explanation.

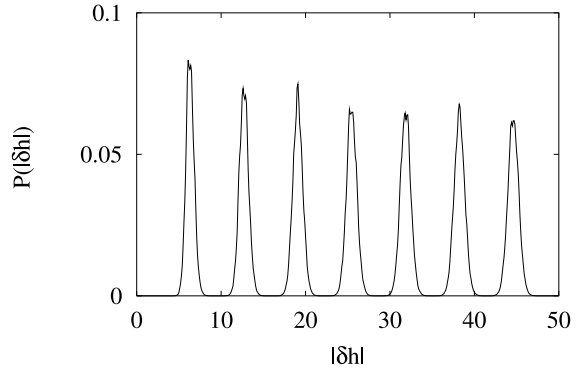


FIG. 10: Distribution of distances between layers in a lamellar stack of 15 layers.

comes questionable, therefore we have compared  $s_{1,2}/s_0$  to the discrete sum obtained by the direct evaluation of (7) and (5), taking into account the periodic boundary conditions. At first sight, the agreement seems reasonable (see Fig. 15). However, the in-plane correlation length  $\xi$  obtained in the fit,  $\xi = 2.6 \pm 0.1 \sigma$ , is significantly larger than that calculated in the big system. Hence one of the phenomenological parameters  $K_c$  or  $B$ , or both, are affected by finite size effects. For example, the effective layer compressibility  $B$  could be reduced in small systems, due to the fact that the layer fluctuations are correlated more strongly (cf. Fig. 10). This would lead to an effective increase of the in-plane correlation length  $\xi$ . Obviously, the finite thickness of the simulated system in the direction of the director affects the fluctuations seriously. In our model, however, a slab thickness of fifteen bilayers seems sufficient to recover the behavior described by DH theory for an infinite slab.

From the parameters  $\eta_1 = 0.053$  and  $\xi = 2.34 \sigma$ , we can calculate the bending energy  $K_c = 4 k_B T$  and

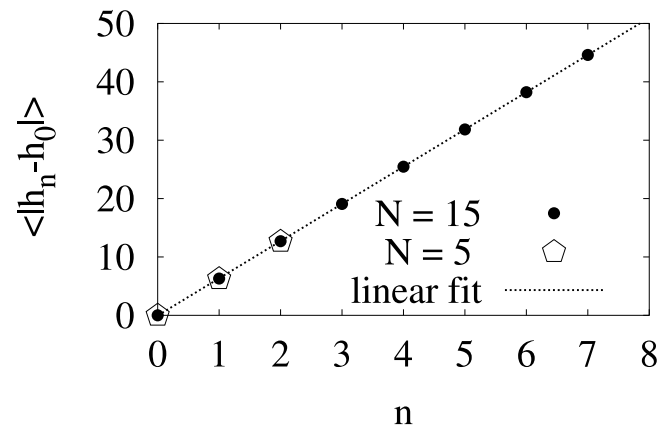


FIG. 11: Mean inter-lamellar distance between bilayers separated by  $n$  solvent layers,  $\langle |h_n(0) - h_0(0)| \rangle$ , vs.  $n$ . The solid line is a linear fit.

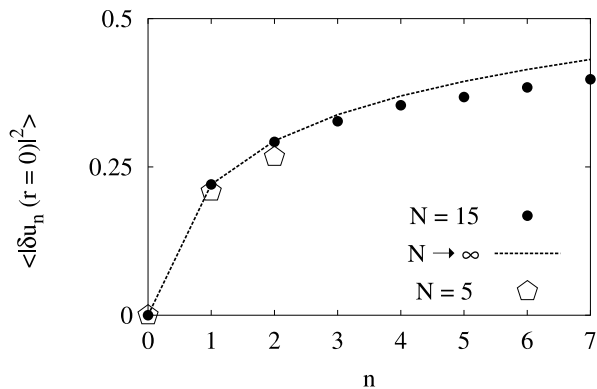


FIG. 12: Variance of the distribution of inter-lamellar distances between bilayers separated by  $n$  layers of solvent. Data are shown for the large system (15 bilayers) and the small system (5 bilayers). The line is the prediction of Eq. (12), using the Caillé parameter  $\eta_1/q_1^2 = 0.055$ .

the compressibility modulus  $B = 0.13 k_B T \cdot \sigma^{-4}$ . Using these elastic constants and the interlamellar distance  $\bar{d} = 6.38 \sigma$ , we can now re-inspect the spectrum  $s_0(q_\perp)$  of correlations within single membranes. It can be compared directly with the theoretical prediction (8), without further fit parameter. The result is shown in Fig. 16. The discrete harmonic theory describes the data well for the large system.

## V. DISCUSSION.

To summarize, we have investigated a bulk lamellar phase in an amphiphilic system by molecular dynamics simulations, using a phenomenological off-lattice model of a binary amphiphile-solvent mixture. The system was studied in the  $(NP_n P_t T)$ -ensemble using an extended Hamiltonian, which ensured that the pressure in the sys-

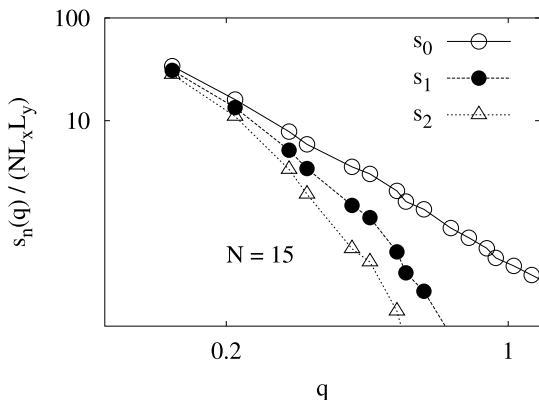


FIG. 13: Membrane correlation spectra  $s_n(q_\perp)/(L_x L_y)$  vs.  $q_\perp$  for the system of 15 bilayers.

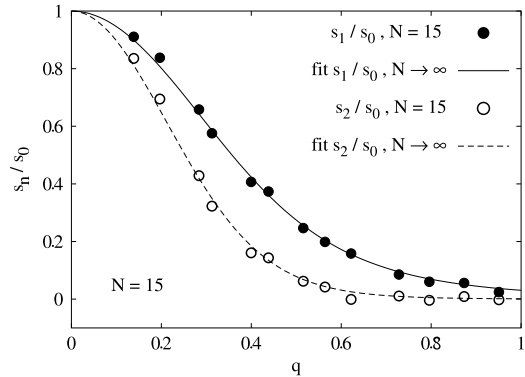


FIG. 14: Ratio  $s_{1,2}(q_\perp)/s_0(q_\perp)$  vs. wave vector  $q_\perp$  in the system with 15 lamellae. The dots represent simulation data, and the solid lines are fits of Eq. (9) with  $X = (\xi q_\perp)^4$  and  $\xi_1 = 2.35 \sigma$ ,  $\xi_2 = 2.33 \sigma$ .

tem was isotropic. Therefore, the membranes had no surface tension.

At high amphiphile concentration, (80% bead percent of amphiphiles), the amphiphilic molecules self-assemble into a lamellar phase, *i.e.*, a stack of bilayers. The distances between the membranes fluctuate in a way that agrees well with the predictions of the discrete harmonic model. From these we could estimate the compressibility modulus  $B$  of the smectic. Furthermore, we have analyzed the in-plane fluctuation spectra of the membranes and extracted the in-plane correlation length  $\xi$ . Our results were in overall good agreement with the predictions of the discrete harmonic theory, down to wavelengths of roughly  $8 \sigma$ .

Fluctuation spectra of free membranes are usually characterized by a scaling law  $s_0(q) \propto q_\perp^4$ . Looking at the data in Fig. 16, we notice that our system does not

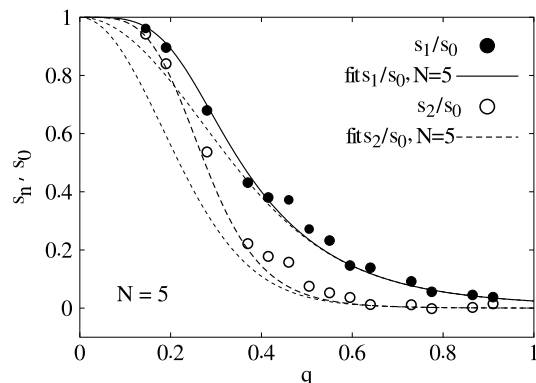


FIG. 15: Ratio  $s_{1,2}(q_\perp)/s_0(q_\perp)$  vs. wave vector  $q_\perp$  in the system with 5 lamellae. The dots represent simulation data, and the solid lines are fits using the discrete summation of Eq. (7) with  $\xi_1 = 2.5 \sigma$ ,  $\xi_2 = 2.7 \sigma$ . Also shown for comparison are the curves obtained with the infinite slab approximation (Eq. (9) and the same values of  $\xi$  (thin lines).

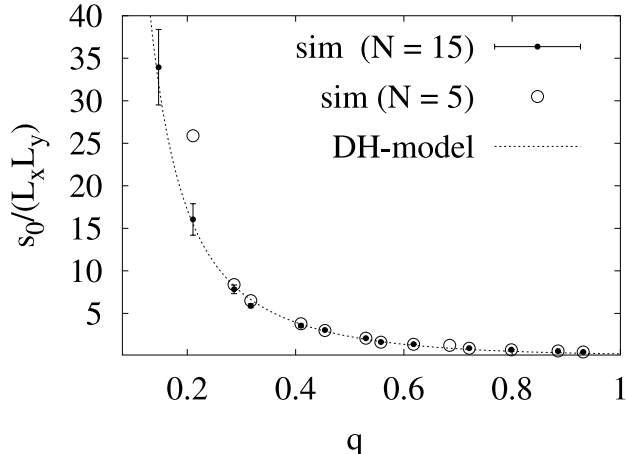


FIG. 16: Autocorrelation spectrum  $s_0(q_\perp)/(L_x L_y)$  of membranes in a stack of 15 layers. The solid line gives the prediction of the elastic theory (8) with the parameters  $B = 0.13 k_B T \sigma^{-4}$  and  $\xi = 2.35 \sigma$ .

exhibit a regime with this scaling. This finding, which was unexpected at first sight, can be rationalized from an analysis of the relevant length scales of the system. The elastic theory (1) predicts free membrane behavior at wave-vectors  $q_\perp \xi \gg 1$ . The membrane fluctuations are then incoherent and dominated by in-plane correlations.

In our system, however, the validity of the continuum approximation (1) breaks down at wave-vectors larger than  $q_\perp \sim \sigma^{-1} \sim \xi^{-1}$ , and the free membrane regime is never observed. The problem lies in the fact that the in-plane correlation length  $\xi$  is of molecular order ( $\xi \sim 2.34 \sigma$ ). We recall that  $\xi$  is closely related to the interactions between membranes, which are characterized by the compressibility modulus  $B$  ( $\xi = (K_c/B)^{1/4}$ ). For free, noninteracting membranes, the correlation length  $\xi$  is infinite. For confined membranes,  $\xi$  becomes finite. In our case, where the lamellae are separated by only a few molecules, ( $\bar{d} \sim 6 \sigma$ ), it is not surprising that  $\xi$  is also of the order of the size of molecules. This explains why incoherent membrane fluctuations cannot be observed in our model.

We can compare our results to those obtained for a lamellar phase which is only stabilized by the Helfrich interactions. Inserting the bending energy  $K_c = 4 k_B T$ , and the membrane thickness  $\bar{t} = 4.4 \sigma$ , one calculates<sup>39</sup>

$$\frac{B}{k_B T} = \frac{9\pi^2}{64} \frac{(k_B T)}{K_c (\bar{d} - \bar{t})^4} = 0.01 \sigma^{-4} \quad (18)$$

$$\eta_1 = \frac{4}{3} \left(1 - \frac{\bar{t}}{\bar{d}}\right)^2 = 0.08 \quad (19)$$

We recall that the real compressibility modulus in our model was given by  $B/k_B T = 0.13 \sigma^{-4}$ , and the real

Caillé parameter by  $\eta_1 = 0.053$ . Thus the Helfrich theory underestimates the stiffness of the interactions between the membranes of our model by one order of magnitude.

### Acknowledgements

We thank Thomas Soddeman, Ralf Everaers and Hong-Xia Guo for stimulating discussions. We thank the Région Rhône-Alpes for subsidizing a generous allocation of computer time on the computing center of the Commissariat à l'Énergie Atomique (Grenoble) within the "conseil des partenaires".

### Appendix A: $(N, P_n, P_t, T)$ algorithm.

Our algorithm was adapted from one published earlier by Kolb *et al.*,<sup>34</sup> which is similar to the piston algorithm proposed by Zhang *et al.*<sup>40</sup> It allows to simulate the lamellar phase in a constant- $(N P_n P_t T)$  ensemble, where  $P_n$  and  $P_t$  are the pressures normal and parallel to the smectic layers. The ability of controlling both  $P_n$  and  $P_t$  was crucial for our simulations, because the properties of smectic structures depend noticeably on the difference between  $P_n$  and  $P_t$ .<sup>9</sup> Since we simulate a part of a bulk lamellar domain, we imposed the same pressure in both directions  $P_n = P_t = P$ .

This was done as follows. As described in the main text, the systems were set up such that the director of the smectic points along the  $z$ -direction of the simulation box. During a simulation run, the director fluctuated only by a few degrees. Thus the normal and tangential pressure were essentially given by the diagonal components of the pressure tensor,  $\mathcal{P}_n = \mathcal{P}_{zz}$  and  $\mathcal{P}_t = (\mathcal{P}_{xx} + \mathcal{P}_{yy})/2$ . Here the pressure tensor is defined as usual

$$\mathcal{P}_{\alpha\beta} = \frac{1}{V} \sum_i \frac{m_i v_i^2}{2} \delta_{\alpha\beta} - \frac{1}{6V} \sum_{i \neq j} \mathbf{f}_{ij}^\alpha \cdot \mathbf{r}_{ij}^\beta, \quad (20)$$

where  $\alpha$  and  $\beta$  are  $x, y$  or  $z$ ;  $V$  is the box volume and the sum  $i, j$  runs over all beads in the system,  $\mathbf{f}_{ij}$  is the force exerted by the bead  $j$  on the bead  $i$ , and  $\mathbf{r}_{ij} = \mathbf{r}_i - \mathbf{r}_j$  is the vector separating the two beads.

The constant pressure ensemble was realized using the extended ensemble method originally suggested by Anderson, Parinello and Rahman.<sup>32,33,34</sup> The dimensions  $L_\alpha$  of the box are taken to be additional degrees of freedom, which contribute to the Hamiltonian with an extra kinetic energy and a potential term. The extended Hamiltonian then reads

$$\mathcal{H}^{ext} = \left\{ \sum_{i,\alpha} \frac{1}{2m} \frac{\pi_{i\alpha}^2}{L_\alpha^2} + \sum_{i,j>i} v_{ij}(|r_{ij}|) \right\} + \left\{ \frac{1}{2Q} \left( \frac{\Pi_y^2}{2} + \Pi_z^2 \right) + P \prod_\alpha L_\alpha \right\} \quad (21)$$

where  $Q$  and  $\Pi_\alpha$  are the mass and the momenta of the box variables, and the other variables refer to the beads:  $m$  is the mass,  $\pi_{i\alpha}$  the momentum of bead  $i$  in the direction  $\alpha$ ,  $r_{ij}$  the distance between beads  $i$  and  $j$ , and  $v_{ij}$  the interaction potential. The Hamiltonian defines equations of motion for  $L_\alpha$  and  $r_{i\alpha}$ , thus the dimensions of the simulation box fluctuate throughout the simulation. This may cause problems in the  $(x, y)$ -plane, where the smectic behaves like a liquid and no mechanism prevents excessive deformations of the simulation box. Therefore we have imposed the constraint that the ratio  $\lambda = L_x/L_y$  remains constant during the simulation.<sup>41,42</sup> The equations of motion derived from this extended Hamiltonian were translated into a symplectic algorithm with the direct translation technique (see *e.g.* Ref. 43).

The constant temperature was realized by means of a Langevin thermostat: We introduced friction forces and a random stochastic force (noise), with relative amplitudes given by the fluctuation dissipation theorem.<sup>34</sup>

An actual molecular dynamics update of the algorithm includes the following steps (the notation is as in Ref. 34:  $\pi_{i\alpha} = m_i v_{i\alpha} L_\alpha$  and  $s_{i\alpha} = r_{i\alpha}/L_\alpha$ ).

1.  $\forall i, \forall \alpha : \pi_{i\alpha} \rightarrow \pi_{i\alpha} + L_\alpha \frac{\Delta t}{2} (\mathbf{F}_i - \frac{\gamma_p}{L_\alpha m_i} \pi_i + \sqrt{k_B T \gamma_p \Delta t} \eta_i(t))$
2.  $\Pi_z \rightarrow \Pi_z + \frac{\Delta t}{2} \frac{V}{L_z} (\mathcal{P}_{zz} - P)$   
 $\Pi_y \rightarrow \Pi_y + \frac{\Delta t}{2} \frac{V}{L_y} [(\mathcal{P}_{yy} + \mathcal{P}_{xx}) - 2P]$
3.  $L_z \rightarrow L_z + \frac{\Delta t}{2} \frac{\Pi_z}{Q}$   
 $L_y \rightarrow L_y + \frac{\Delta t}{2} \frac{\Pi_y}{2Q}$   
 $L_x \rightarrow \lambda L_y$
4.  $\forall i, \forall \alpha : s_{i\alpha} \rightarrow s_{i\alpha} + \frac{\Delta t}{L_\alpha^2 m_i} \pi_{i\alpha}$
5. Same as 3.
6. Calculate new forces and new pressure tensor.
7. Same as 2.
8. Same as 1.

We have used the following parameters:  $Q = 0.1 m$ ,  $\Delta t = 0.005 \tau$ ,  $\gamma_p = 1.0 m \cdot \tau^{-1}$ ,  $T = 1.0 \epsilon/k_B$ . The time step  $\Delta t = 0.005 \tau$  was small enough that no bonds could break during the simulation.

## Appendix B: Spatial spectral analysis

This appendix describes how we determined the local positions of membranes in the lamellar stack.

1. The space is divided into  $N_x N_y N_z$  cells of size  $(dx, dy, dz)$  with  $N_x = N_y = 32$ . For a density of 0.85 particle per volume unit,  $dx = dy \simeq 1.3 \sigma$  and  $dz \simeq 1.0 \sigma$ . The size of cells may vary from one configuration to another because the dimensions of the box dimensions vary.
2. The relative density of tail beads in each cell is calculated as the ratio  $\rho_{tail}(x, y, z) = N_{tail}(x, y, z)/N_{tot}(x, y, z)$  of the number of tail beads  $N_{tail}(x, y, z)$  and the total number of particles  $N_{tot}(x, y, z)$ .
3. The membranes are defined as the space where the relative density of tail beads is higher than a threshold ( $\rho_{tail}(x, y, z) > \rho_0$ ). The choice of the threshold depends on the mesh size in  $x$ - and  $y$ - directions ( $dx = L_x/N_x$  and  $dy = L_y/N_y$ ). Typically, we used 0.65 to 0.75 (80 % of the maximum relative density of tail beads).
4. The cells that belong to membranes are associated into clusters: Two membrane cells that share at least one vortex are attributed to the same cluster. Each cluster defines a membrane. This algorithm identifies membranes even if they have holes. At the presence of necks between adjacent membranes (local fusion), additional steps have to be taken. But this happened very rarely in our system.
5. For each membrane  $n$  and each position  $(x, y)$ , the two heights  $h_n^{min}(x, y)$  and  $h_n^{max}(x, y)$  where the density  $\rho_{tail}(x, y, z)$  equals the threshold  $\rho_0$  are estimated by a linear extrapolation. The mean position and the thickness are then defined by
 
$$h_n(x, y) = \frac{1}{2} [h_n^{max}(x, y) + h_n^{min}(x, y)]$$

$$t_n(x, y) = \frac{1}{2} [h_n^{max}(x, y) - h_n^{min}(x, y)] \quad (22)$$
 If the membrane happens to have a hole at  $(x, y)$ , we attribute the mean position  $\bar{h}_n$  to  $h_n(x, y)$  ( $h_n^{hole}(x, y) = \bar{h}_n$ ). If two neighboring membranes  $i$  and  $j$  are connected by a neck at  $(x, y)$  (local fusion), both membrane positions are taken to be at  $h_{i,j}^{neck}(x, y) = [h_i^{max}(x, y) + h_j^{min}(x, y)]/2$ .
6. The functions  $u_n(x, y) = h_n(x, y) - \bar{h}_n$  are calculated and Fourier transformed in the  $x$  and  $y$  dimension as defined by the Eq. (3), giving  $u_n(q_x, q_y)$ . The correlation functions  $s_n(q_x, q_y)$  are calculated via Eq. (7). The radial average of  $s_n(q_x, q_y)$ ,  $s_n(q_\perp)$ , is performed by binning over wave-numbers on a grid which does not depend on the dimension of the box. Ensemble averages were carried out for  $s_n(q_\perp)$  ( $n = 0, 1, 2$ ).

- 
- \* Electronic address: claire@cecam.fr  
† Electronic address: schmid@physik.uni-bielefeld.de
- <sup>1</sup> A. Caillé, *Rapports de l'Académie des Sciences* **274B**, 891 (1972).
  - <sup>2</sup> P. G. de Gennes and J. Prost, *The Physics of Liquid Crystals* (Oxford University Press, London, 1993).
  - <sup>3</sup> N. Lei, C. R. Safinya, and R. F. Bruinsma, *J. Phys. II* **5**, 1155 (1995).
  - <sup>4</sup> G. Bouglet and C. Ligoure, *Eur. Phys. J. B* **9**, 137 (1999).
  - <sup>5</sup> M. Müller and M. Schick, *J. Chem. Phys.* **105**, 8282 (1996).
  - <sup>6</sup> R. Goetz, G. Gompper, and R. Lipowsky, *Phys. Rev. Lett.* **82**, 221 (1999).
  - <sup>7</sup> A. Werner, M. Müller, F. Schmid, and K. Binder, *Phys. Rev. E* **59**, 728 (1999).
  - <sup>8</sup> A. Werner, M. Müller, and F. Schmid, *J. Chem. Phys.* **110**, 5370 (1999).
  - <sup>9</sup> S. J. Marrink and A. E. Mark, *J. Chem. B* **105**, 6122 (2001).
  - <sup>10</sup> R. Holyst, *Phys. Rev. A* **44**, 3692 (1991).
  - <sup>11</sup> P. M. Chaikin and T. C. Lubenski, *Principles of Condensed Matter Physics* (Cambridge University Press, London, 1995).
  - <sup>12</sup> S. Chandrasekhar, *Liquid crystals* (Cambridge University Press, London, 1977).
  - <sup>13</sup> S. A. Safran, *Statistical Thermodynamics of Surfaces, Interfaces, and Membranes* (Addison-Wesley Publishing Company, Reading, Massachusetts, 1994).
  - <sup>14</sup> H. I. Petrache, N. Goulaiev, S. Tristam-Nagle, R. Zhang, R. M. Suter, and J. F. Nagle, *Phys. Rev. E* **57**, 7014 (1998).
  - <sup>15</sup> Y. Lyatskaya, Y. Liu, S. Tristam-Nagle, J. Katsaras, and J. F. Nagle, *Phys. Rev. E* **63**, 011907 (2001).
  - <sup>16</sup> G. S. Grest and K. Kremer, *Phys. Rev. A* **33**, 3628 (1986).
  - <sup>17</sup> K. Kremer, G. S. Grest, and I. Carmesian, *Phys. Rev. Lett.* **61**, 566 (1988).
  - <sup>18</sup> K. Kremer and G. S. Grest, *J. Chem. Phys.* **92**, 5057 (1990).
  - <sup>19</sup> T. Soddemann, B. Dünweg, and K. Kremer, *Eur. Phys. J. E* **6**, 409 (2001).
  - <sup>20</sup> H. X. Guo, K. Kremer, and T. Soddemann, *Phys. Rev. E* **66**, 061503 (2002).
  - <sup>21</sup> R. Goetz and R. Lipowsky, *J. Chem. Phys.* **108**, 7397 (1998).
  - <sup>22</sup> S. J. Marrink, E. Lindhal, O. Edholm, and A. E. Mark, *J. Am. Chem. Soc.* **123**, 8638 (2001).
  - <sup>23</sup> J. C. Shelley, M. Y. Shelley, R. C. R. S. Bandyopadhyay, and M. L. Klein, *J. Phys. Chem. B* **105**, 4464 (2001).
  - <sup>24</sup> J. C. Shelley, M. Y. Shelley, R. C. Reeder, S. Bandyopadhyay, P. B. Moore, and M. L. Klein, *J. Phys. Chem. B* **105**, 9785 (2001).
  - <sup>25</sup> Y. Lansac, M. A. Glaser, and N. A. Clark, *Phys. Rev. E* **64**, 051703 (2001).
  - <sup>26</sup> M. Yoshida, N. Seo, K. Hori, and H. Toriumi, *Mol. Cryst. Liq. Cryst.* **365**, 1769 (2001).
  - <sup>27</sup> R. Netz and M. Schick, *Phys. Rev. E* **53**, 3875 (1996).
  - <sup>28</sup> M. Müller, K. Katsov, and M. Schick, *J. Chem. Phys.* **116**, 2342 (2002).
  - <sup>29</sup> R. G. Larson, *J. Phys. II* **6**, 1441 (1996).
  - <sup>30</sup> A. Ciach, *J. Chem. Phys.* **93**, 5322 (1990).
  - <sup>31</sup> P. H. Nelson, G. C. Rutledge, and T. A. Hatto, *J. Chem. Phys.* **107**, 10777 (1997).
  - <sup>32</sup> H. C. Andersen, *J. Chem. Phys.* **72**, 2384 (1980).
  - <sup>33</sup> M. Parrinello and A. Rahman, *Phys. Rev. Lett.* **45**, 1196 (1980).
  - <sup>34</sup> A. Kolb and B. Dünweg, *J. Chem. Phys.* **111**, 4453 (1999).
  - <sup>35</sup> H. X. Guo and K. Kremer, *J. Chem. Phys.* **118**, 7714 (2003).
  - <sup>36</sup> H. X. Guo and K. Kremer, 2003.
  - <sup>37</sup> H. X. Guo, 2002, private communication.
  - <sup>38</sup> D. C. Morse and S. T. Miller, *Phys. Rev. E* **47**, 1119 (1993).
  - <sup>39</sup> D. Roux and C. R. Safinya, *J. Phys. (France)* **49**, 307 (1988).
  - <sup>40</sup> Y. Zhang, S. E. Feller, R. W. Pastor, and B. R. Brook, *J. Chem. Phys.* **103**, 4613 (1995).
  - <sup>41</sup> K. M. Aoki and F. Yonezawa, *Phys. Rev. A* **46**, 6541 (1992).
  - <sup>42</sup> H. Dominguez, E. Velosco, and J. A. Alejandre, *Mol. Phys.* **100**, 2739 (2002).
  - <sup>43</sup> M. E. Tuckerman and G. J. Martyna, *J. Phys. Chem. B* **104**, 159 (2000).